Journal of Intelligent Manufacturing and Special Equipment

181

# Deformation simulation analysis and validation for large long-length-to-diameter ratio thin-walled cylindrical parts heat treatment

Xiaojuan Zhang, Lu Bai, Lijun Xu, Jingtao Liu, Zhongping Zhou, Rui Li, Lijian Zhu and Junxi Wang
*Shanghai Space Propulsion Technology Research Institute, Shanghai, China, and*
Ziyi Song and Chongjun Wu
*College of Mechanical Engineering, Donghua University, Shanghai, China*

Received 16 May 2025
Revised 26 May 2025
Accepted 9 June 2025

## Abstract

**Purpose** – Thin-walled cylindrical structures with large length-to-diameter ratios in the aerospace industry are vulnerable to deformation during manufacturing and heat treatment, which may cause product failure and affect equipment service life. This study aims to analyze the deformation of such cylinders during heat treatment correction and improve correction accuracy.

**Design/methodology/approach** – A 3D point cloud scanning reconstruction technology-based method is proposed for efficient cylinder measurement. Finite element analysis (FEA) is employed to simulate the quenching process in heat treatment correction. The visual analysis results from the point cloud are compared with the simulated cylinder deformation rebound data, and the simulation model is refined through multiple verification steps.

**Findings** – The refined simulation model enables accurate prediction and analysis of deformation rebound, significantly improving the correction accuracy. The simulation and experimental data show a high degree of agreement, indicating that the simulation can effectively predict the deformation rebound.

**Originality/value** – The integration of 3D point cloud scanning technology and finite element simulation provides a new approach for the deformation analysis of large-length-to-diameter thin-walled cylinders during heat treatment correction, offering valuable guidance for practical production processes.

**Keywords** Point cloud preprocessing, Efficient measurement, Tempering simulation, Deformation prediction

**Paper type** Research paper

## 1. Introduction

Thin-walled cylinders with large length-to-diameter ratio are commonly applied in the aerospace industry for manufacturing certain shell components. Due to the unique working conditions and requirements of these components under extreme conditions such as high temperatures, high pressures, and high-speed airflow, the components must possess high strength, heat resistance, and impact resistance to ensure the proper operation of core spaceflight parts in complex environments (Wang *et al.*, 2022). Thin-walled cylindrical structures are characterized by their lightweight nature, high axial compressive stiffness and strength, high resistance to lateral bending, and excellent energy absorption both axially and laterally. These features make them widely applicable in engineering fields such as vehicle collision safety systems, offshore platforms (Rong *et al.*, 2018), aircraft cabins, and pipelines



Journal of Intelligent Manufacturing and Special Equipment
Vol. 6 No. 2, 2025
pp. 181-197
Emerald Publishing Limited
e-ISSN: 2633-660X
p-ISSN: 2633-6596
DOI 10.1108/JIMSE-05-2025-0007

(Fan *et al*., 2024; Lu *et al*., 2024; Zhou *et al*., 2023). Thin-walled cylinders are manufactured through processes such as spinning, electron beam welding, and heat treatment. These processes can induce deformation and residual stress in the material. During heat treatment and quenching, the cumulative effects of deformation and stress tend to localize and release, often leading to significant distortions in the shell during quenching. These distortions typically manifest as radial ellipticity, bending, twisting, etc. Therefore, the manufacturing and deformation analysis of thin-walled cylinders with large length-to-diameter ratio is particularly critical. Moreover, these shells are typically made from ultra-high-strength steel, and their material properties are enhanced through processes such as heat treatment (e.g. quenching and tempering) during the shell-forming process (Lassi *et al*., 2021; Keränen *et al*., 2022). However, during heat treatment, the components may experience deformation (Hannula *et al*., 2019; Esterl *et al*., 2019). As a result, developing efficient correction methods is essential.

For large-length-to-diameter thin-walled cylindrical components, with a significant length-to-diameter ratio and rotational symmetry (360°), manufacturing processes such as spinning, electron beam welding, and heat treatment are commonly used. These processes inevitably lead to deformation, severely affecting the performance of the components. The current correction method commonly used for this type of cylinder is the tempering correction process. This method relies on the high plasticity during the tempering process, applying pressure to correct the deformation. The tempering correction method typically includes inner support and outer hoop types. For thin-walled cylinders, the outer hoop correction is generally preferred. After quenching, ultra-high-strength steel exhibits increased hardness and reduced plasticity (Mishnev *et al*., 2023; Tian *et al*., 2022). To correct deformation after quenching, the component is tempered together with a jig, utilizing the transformation in microstructure and the associated enhancement of plasticity during tempering to achieve the desired shape correction (Zhang *et al*., 2019).Current shaping and measurement methods do not meet the increasing technical requirements of products. Existing roundness measurement and correction methods are inefficient, and the collection of original data before and after heat treatment is often incomplete. Moreover, the measurement and determination of the cylinder's correction position are currently performed manually. This method places high demands on the experience and technical skill of the operators, leading to the risk of human error and discrepancies between the corrected and expected results. According to statistics, the qualification rate for a single tempering process is only 61.2%. To ensure qualification, roundness must be continually measured, and when the standard is not met, a second correction must be performed until the radial roundness reaches the qualified standard of $\leq$1.8 mm. This approach not only reduces efficiency but also increases production costs and causes a waste of resources and funds. Therefore, there is an urgent need for a more efficient and accurate method for measuring and correcting thin-walled cylinders.

To address the challenges identified in the previous section, this paper proposes 3D point cloud technology to obtain the geometric data of the cylinder and a method for determining roundness errors through point cloud preprocessing. Given the large volume of point cloud data and the significant noise present, preprocessing is essential to facilitate subsequent data usage (Li *et al*., 2023a). The preprocessing primarily involves noise reduction and filtering (Li *et al*., 2023b; Pei *et al*., 2023), with the aim of minimizing data size and effectively removing noise while preserving the critical characteristics of the component. Subsequently, finite element analysis (FEA) software is used to simulate the correction process and predict the deformation before and after shaping (Li *et al*., 2025; Li *et al*., 2016; Xu *et al*., 2018). As the simulation trials increase, continual adjustments allow the results to closely match the real data. This enables accurate prediction of the deformation before correction, enhancing production efficiency, reducing time and costs, and offering significant guidance for the future development of automation.

This paper specifically focuses on the deformation correction of large-length-to-diameter thin-walled cylinders during heat treatment. It proposes an efficient measurement method based on 3D point cloud scanning technology, combined with finite element simulation

software, to model the quenching-induced correction process of the cylinder. The process begins with scanning the part using a 3D scanner. The resulting point cloud data undergoes preprocessing, including denoising, filtering, and compression techniques. The preprocessed model is then imported into for simulation of the correction process. By setting the temperature field and the pressure applied by the jigs, the simulation predicts the deformation rebound of the cylinder during tempering. The accuracy of the simulation model is verified by comparing the simulation results with actual experimental data, and the model is fine-tuned based on these comparisons. Ultimately, this approach facilitates the optimization of the correction process and enables accurate predictions of deformation outcomes.

## 2. Model setup

### *2.1 Main processes*

To address the challenges of cylinder correction outlined above, this paper proposes a more efficient and accurate correction method. The specific process flow is shown in Figure 1. The main steps are as follows:

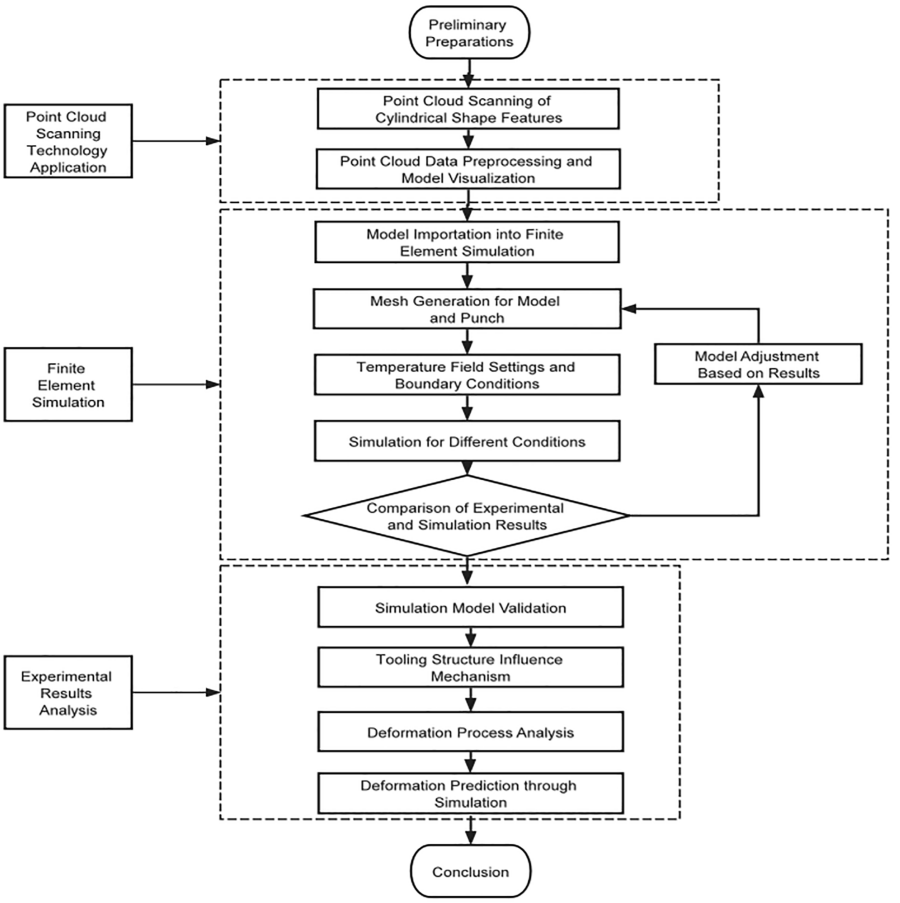


**Figure 1.** Workflow diagram of modeling and simulation study for thin-walled cylindrical parts with a large length-to-diameter ratio. Source: Authors' own work

STEP 1: Modeling the Cylinder Using Point Cloud Scanning Technology: A 3D scanner is used to collect point cloud data of the cylinder. The data is then preprocessed, including steps such as data filtering, denoising, segmentation, compression, and surface reconstruction, to build the 3D model of the cylinder.

STEP 2: Finite Element Simulation of Cylinder Correction Using: The obtained 3D cylinder model is imported into finite element simulation software for preprocessing. The preprocessing steps include material assignment, mesh generation, constraint and load setup, and temperature field configuration. The post-processing stage involves simulating the tempering process under various conditions.

STEP 3: Experimental Data Analysis: The real experimental data is compared with the simulation results to validate the model's accuracy. Additionally, the impact of the jig structure on the results is analyzed, and the deformation process is examined. Finally, the simulation data is fitted to assist in predicting the correction outcomes for future applications.

*2.2 Object description*

The experimental object of this study is a large-length-to-diameter thin-walled cylinder. The cylinder has a length of 1,500 mm, a diameter of 160 mm, and the length-to-diameter ratio greater than 9, with a wall thickness of 1.35 mm. It is a typical large-length-to-diameter thin-walled component, as shown in the 3D model in Figure 2. The specific physical properties of the materials are listed in Table 1. In addition, this material offers good toughness and weldability, with a relatively simple heat treatment process that does not require preheating. It also exhibits stable welding performance and low sensitivity to stress corrosion cracking. The deformation's extent and pattern are mainly determined by quenching process parameters, thermal expansion/contraction, microstructural changes during quenching, machining processes, applied stresses, and product structures. This component is primarily applied in aerospace shell fields. Owing to its precision and manufacturing demands, controlling its roundness and straightness to minimize deformation is crucial. Roundness error, which effectively combines roundness and straightness, is used as a comprehensive indicator to

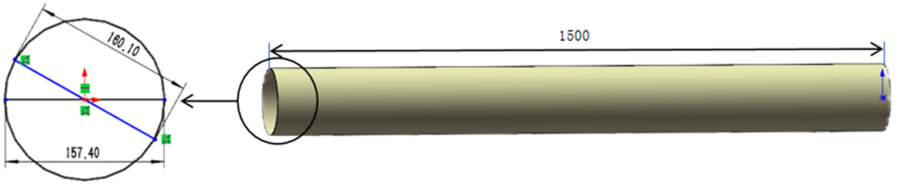


**Figure 2.** Partial 3D model of the spun cylindrical part. Source: Authors' own work

**Table 1.** Material properties for 30Cr3SiNiMoVA ultrahigh-strength steel

| Material property | Parameter |
|---|---|
| Thermal conductivity | 45 W/(m·K) |
| Density | $7.8 \times 10^{-9}$ kg/m$^3$ |
| Young's modulus | 210 GPa |
| Poisson's ratio | 0.3 |
| Coefficient of thermal expansion | $1.13 \times 10^{-5}$ |
| Specific heat capacity | $4.6 \times 10^{8}$ J/(kg·K) |

**Source(s):** Authors' own work

measure the overall deformation of the shell, as it clearly reflects the deviation between the actual shell and the ideal cylindrical shape.

*2.3 Point cloud processing and surface reconstruction*

Point cloud data is a collection of points in three-dimensional space, containing rich spatial information that can be used to display object characteristics and enable visual analysis. Point cloud preprocessing plays a crucial role in the entire point cloud processing pipeline. Preprocessing improves the quality of the point cloud data, reduces computational complexity, and provides a solid data foundation for further processing (Yang *et al*., 2024; Zhu *et al*., 2022; Wang *et al*., 2024). Since there are irrelevant data points in the scanned point cloud data such as sensor mounting brackets, small object features, etc., as shown in the Figure 3(a), the first step is to filter the point cloud data to exclude the points with this large error, i.e. denoising and filtering the data. The core idea of Gaussian filtering is to use a Gaussian function as the convolution kernel and perform convolution with the original point cloud data to smooth the data. The weight of the Gaussian filter is determined by the Gaussian distribution function (normal distribution), which is given by the following Equation (1):

$$G(\mathrm{x}) = \frac{1}{\sqrt{2\pi\sigma^2}} \exp\left(-\frac{\mathrm{x}^2}{2\sigma^2}\right) \tag{1}$$

Where: x is the distance from the data point to the center point. σ is the standard deviation of the Gaussian distribution, controlling the width of the filter and determining the degree of smoothing. G(x) is the corresponding weight. In point cloud processing, a three-dimensional Gaussian function is typically used for filtering. The formula is given by Equation (2):

$$G(\mathrm{p}) = \frac{1}{(2\pi\sigma^2)^{3/2}} \exp\left(-\frac{\|\mathrm{p}\|^2}{2\sigma^2}\right) \tag{2}$$

Where: P is the point in the point cloud. ||p|| is the Euclidean distance between the point and the center point.Gaussian filtering has the advantages of good smoothing effect, continuity, and adaptability (Zheng *et al*., 2022; Zhang *et al*., 2022), and by denoising and filtering the cylinder, the Figure 3(b) can be obtained. Secondly, the point cloud data is down sampled to reduce the point cloud density to reduce the computational cost and accelerate the subsequent processing, and the surface reconstruction of the obtained point cloud data is carried out as shown in Figure 3(c) and (d), respectively, and the processed point cloud data is finally obtained. The entire point cloud preprocessing process is shown in Figure 3 below.

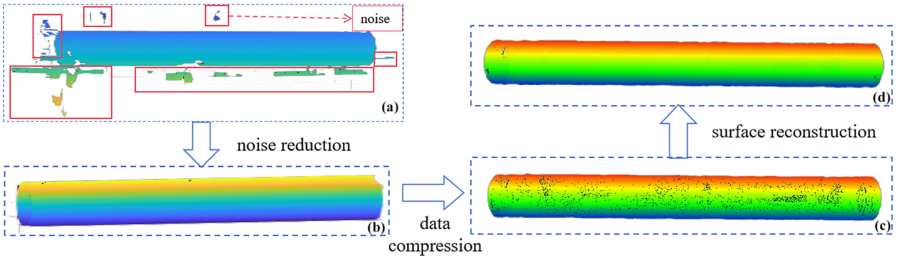


**Figure 3.** Point cloud preprocessing workflow diagram. Source: Authors' own work

*2.4 Finite element simulation model development*

This study uses software to conduct finite element simulations of the cylinder. In practice, there are three primary types of jigs used for cylinder correction: the semicircular jig, the 45-degree jig, and the flat-plate jig. Each of these jigs has its advantages. During the actual correction process, the cylinder deformation varies, and the heat treatment requirements differ depending on the model. Based on these considerations, the correction process can be divided into three types: (1) roundness correction, (2) roundness and straightness correction, and (3) roundness and roundness runout correction. The jig selection is based on the deformation trend of the workpiece. For the first two cases, a semicircular or 45-degree jig is selected, while for roundness and roundness runout correction, roundness is corrected first. If the roundness is not up to standard, additional roundness correction is performed. After roundness meets the required standard, if the roundness runout still does not meet the requirement and the high and low points differ by 135° or less, a flat-plate jig is used. These three types of jigs are capable of correcting the majority of workpieces.

Since the quenching process causes the cylinder to deform, resulting in a non-standard cylindrical shape, it is essential to determine the contact area between the jig and the cylinder. Taking the 45-degree jig as an example, the schematic diagram in Figure 4 shows that the light blue ellipse represents the deformed cylinder cross-section after quenching, and the dark blue circle represents the target shape. The red dashed block represents the jig's support block. When the 45-degree jig's support block just touches the cylinder, the position is shown by the red dashed block 1 and the light blue ellipse in the diagram. It can be seen that the contact range is a single point. Based on the experience of reverse deformation correction and rebound, assuming a cylinder deformation of 2 mm, the required downward pressure is 4 mm. After applying this downward pressure, the jig's contact area increases significantly, as shown by red dashed block 2 and the dark blue ellipse. The maximum contact area between the jig and the cylinder is 38 mm × 50 mm. In the simulation, the contact area is set to 38 mm × 50 mm. For the other two types of jigs, similar calculations yield contact areas of 56 mm × 50 mm for the semicircular jig and 148 mm × 50 mm for the flat-plate jig. Thus, the pressure application for different jigs can be simplified to the block models shown in Figure 5, where model (a) represents the 45-degree jig equivalent, and model (b) represents the semicircular jig equivalent.

The quality of the mesh directly affects the accuracy of the finite element results. For the cylinder model, a hexahedral mesh is used, resulting in 63,096 elements. The pressure block model uses the same method, with 2,194 elements (Zhuang *et al.*, 2024; Li *et al.*, 2024). Schematic diagram of cylinder model meshing and constraint setting are shown in Figure 6. During the actual tempering process, the cylinder is clamped into the jig and heated in a furnace for 2 h, with the setup placed vertically. To analyze the structural deformation during

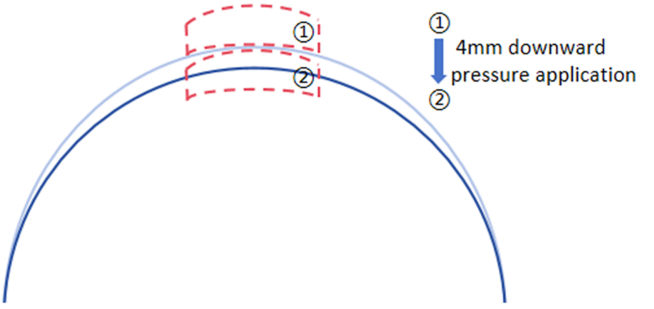


**Figure 4.** Schematic of jig and cylinder contact area calculation. Source: Authors' own work

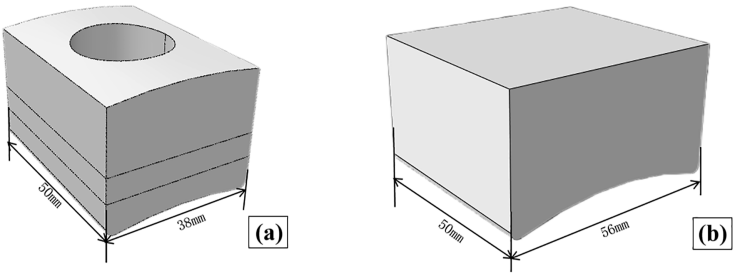


**Figure 5.** Pressure block models: (a) 45-degree jig equivalent; (b) semicircular jig equivalent. Source: Authors' own work

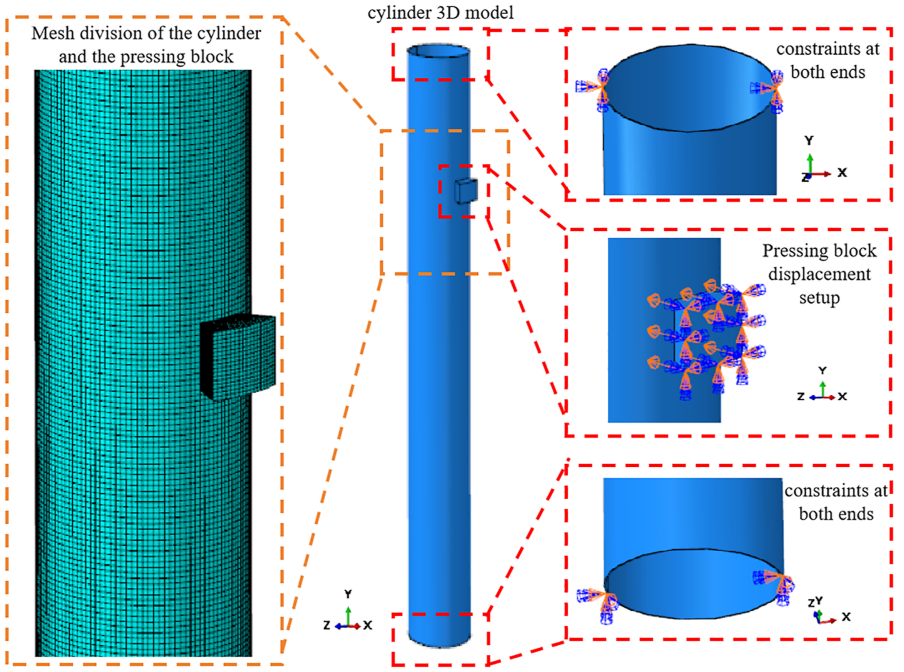


**Figure 6.** Schematic diagram of cylinder model meshing and constraint setting. Source: Authors' own work

the heat treatment, the analysis type in the simulation is set to thermostructural coupling. Three analysis steps are used, with specific parameters shown in Table 2. The workpiece is constrained at both ends, and the pressure applied by the pressure block to the cylinder is a downward force along the *y*-axis.

The rebound of the cylinder after correction depends on factors such as the material type, material microstructure, temperature, and the applied downward pressure. In this study, the material under consideration is 30Cr3, with consistent material conditions after quenching. Thus, the rebound is directly related to the amount of downward pressure applied and the contact area during correction. To reduce experimental efforts and save costs, this study combines simulations and process experiments. The downward pressure and contact area are chosen as independent variables, while the rebound amount is the dependent variable. Since

**Table 2.** Specific parameters for the three analysis steps in the simulation

| | Step 1 | Step 2 | Step 3 |
|---|---|---|---|
| Interaction type | Surface-to-surface contact | Surface heat exchange | Surface radiation |
| Total analysis time (s) | 1 | 300 | 300 |
| Environment temperature (°C) | 20 °C | 300 °C | 20 °C |

**Source(s):** Authors' own work

the qualification standard for this model is roundness runout ≤1.8 mm, with deformation ranging from 1.8 to 3 mm, the downward pressure is set in 0.1 mm increments from 1.8 to 3 mm, with 13 sets in total. The contact area is divided into two types: 45° jig and semicircular jig. The flat-plate jig is not considered, as it is used only in secondary correction. The correction simulation experiment is divided into two groups, as shown in Table 3. By combining experimental and simulation data, the correction process can be analyzed and optimized.

## 3. Results and discussion

### *3.1 Simulation model verification*

In the actual production process, the cylinder deformation correction involves heating the workpiece in a furnace to around 300 °C and maintaining this temperature for 2 h. Prior to heating, the correction jig is clamped onto the cylinder, and both the jig and cylinder are heated together. As shown in Figure 7, the use of adjustable calibration tooling involves adjusting the tooling position based on data from point cloud reconstruction analysis to ensure precise correction of cylinder deformation, thereby significantly enhancing the qualification rate of cylinder calibration. The tooling is suitable for cylinders with large diameters and significant deformations and can be adapted to various specifications of cylinders. A pad should be placed between the cylinder and the tooling to prevent the cylinder structure from being compromised by clamping forces.

**Table 3.** Experimental data for the 45-degree tool setup

| Experiment number (45° tool) | Downward displacement (mm) | Experiment number (semi-circular tool) | Downward displacement (mm) |
|---|---|---|---|
| 1 | 1.8 | 1 | 1.8 |
| 2 | 1.9 | 2 | 1.9 |
| 3 | 2 | 3 | 2 |
| 4 | 2.1 | 4 | 2.1 |
| 5 | 2.2 | 5 | 2.2 |
| 6 | 2.3 | 6 | 2.3 |
| 7 | 2.4 | 7 | 2.4 |
| 8 | 2.5 | 8 | 2.5 |
| 9 | 2.6 | 9 | 2.6 |
| 10 | 2.7 | 10 | 2.7 |
| 11 | 2.8 | 11 | 2.8 |
| 12 | 2.9 | 12 | 2.9 |
| 13 | 3 | 13 | 3 |

**Source(s):** Authors' own work

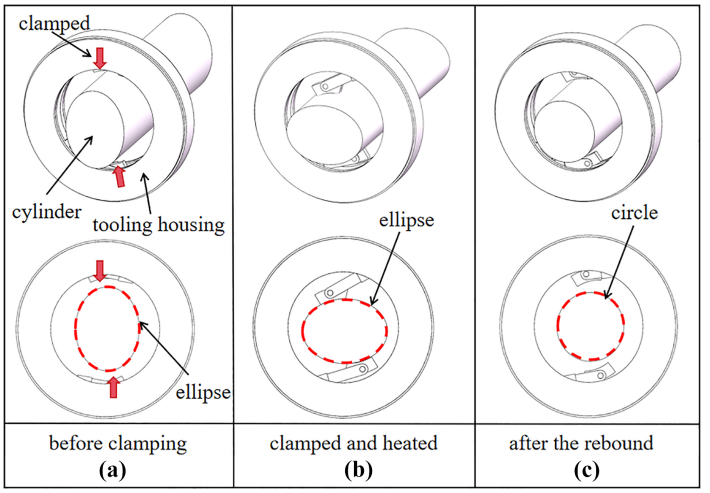


**Figure 7.** Schematic diagram of cylinder before and after clamping. Source: Authors' own work

After the cylinder maintains the desired temperature, the jig is removed, and the cylinder is allowed to cool to room temperature. The roundness runout of the cylinder is then measured to obtain a set of experimental data. To clearly present the variation trend of the rebound amount in both simulation and experimental data as a function of the applied downward pressure, a line chart was used for visual analysis, as shown in Figure 8. Line charts are particularly effective in visually displaying the relationship between two variables, making them ideal for analyzing the correlation between simulation and experimental data. In the chart, the *x*-axis represents the downward pressure, and the *y*-axis represents the rebound amount. It is evident that both the experimental and simulated rebound amounts increase with increasing downward pressure.

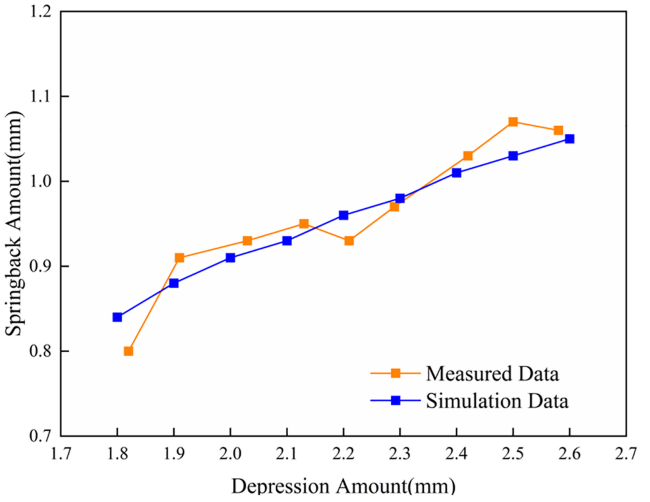


**Figure 8.** Variation of rebound amount with downward pressure: experimental vs. simulation data. Source: Authors' own work

Additionally, a visual inspection reveals that the trends in the simulation data closely match those in the experimental data.

To quantitatively evaluate the consistency between the simulation data and experimental data, a correlation analysis was performed. For instance, in the fatigue life prediction of automotive components, the accuracy of simulation data directly influences design optimization and service life evaluation. Therefore, correlation analysis is crucial for verifying the reliability of the simulation model. Pearson's correlation coefficient is commonly used in correlation analysis due to its precision in measuring linear relationships. It takes values in the range of [−1, 1], making it intuitive to understand. It also has excellent mathematical properties, being symmetric and closely related to linear regression. Pearson's correlation coefficient is widely applied in various disciplines and is a powerful tool for analyzing variable relationships. It is computed based on the covariance and standard deviations of the data, using the formula:

$$r = \frac{\sum_{i=1}^{n}\left(x_i - \overline{x}\right)\left(y_i - \overline{y}\right)}{\sqrt{\sum_{i=1}^{n}\left(x_i - \overline{x}\right)^2 \sum_{i=1}^{n}\left(y_i - \overline{y}\right)^2}} \tag{3}$$

Where $x_i$ and $y_i$ are the sample values of the experimental and simulation data, and $\overline{x}$ and $\overline{y}$ are their respective means. n is the number of samples.

After the analysis of the two sets of data, the following Table 4 data can be obtained, the Pearson correlation coefficient was calculated to be 0.948 indicating a strong positive correlation between the simulation and experimental data, thus confirming the high reliability of the simulation model.

*3.2 Analysis of jig structure influence*

The contact area between different jigs and the cylinder varies, and to explore how different jigs affect the deformation correction results, simulation experiments were conducted using equivalent pressure blocks of the 45-degree and semicircular jigs. In these simulations, the downward pressure depth was controlled to remain constant to ensure accurate and reliable results. As shown in Figure 9, both jigs exhibit an increase in rebound amount as the downward pressure increases. However, at the same downward pressure, the rebound amount with the 45-degree jig is smaller than that with the semicircular jig.

The different rebound amounts during the tempering process can primarily be attributed to the size of the contact area between the pressure block and the cylinder. When the contact area is larger, the stress is distributed more uniformly across the cylinder's surface, causing plastic deformation to occur over a larger area. This leads to the storage of more elastic strain energy within the material. After the tempering correction, the stored elastic strain energy is released, driving the rebound and causing a larger amount of rebound. Additionally, the larger contact area generates more friction, which resists the rebound to some extent. However, this friction

**Table 4.** Pearson correlation coefficient calculation data

| | Mean | Standard deviation (SD) | Total sum | Minimum | Maximum |
|---|---|---|---|---|---|
| Simulation | 0.9544 | 0.0609 | 8.59 | 0.84 | 1.05 |
| Experimental | 0.9611 | 0.0616 | 8.65 | 0.8 | 1.07 |

**Source(s):** Authors' own work

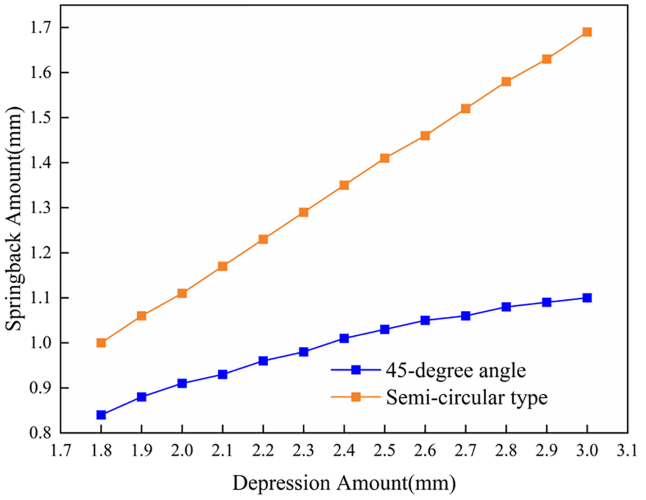


**Figure 9.** Rebound amount variation for 45-degree and semicircular jigs. Source: Authors' own work

also constrains the cylinder's deformation, disturbing the stability of the corrected shape and contributing to the increased rebound.

Conversely, when the contact area is smaller, stress is concentrated in a localized area, causing the material in that region to quickly reach its yield strength and undergo plastic deformation, while the surrounding material undergoes little plastic deformation. Consequently, the amount of stored elastic strain energy is lower, resulting in a weaker rebound driving force. Moreover, the friction in the case of smaller contact areas is also lower, causing less disturbance to the cylinder's shape, making it easier to maintain the corrected shape, which results in a smaller rebound amount. Additionally, the smaller contact area produces a smaller thermal influence zone, meaning that the thermal stress is more localized, and its impact on the overall deformation of the cylinder is limited.

In summary, comparing the two contact areas, a smaller contact area results in less localized elastic strain energy storage, less friction interference, and a more concentrated thermal influence zone. As a result, the rebound amount after tempering correction is significantly smaller than when a larger contact area is used.

### *3.3 Deformation process analysis*

From the perspective of material properties, tempering can adjust the mechanical properties of a material, such as hardness, strength, and plasticity. During tempering, residual stresses within the material are relieved. When the cylinder deforms during quenching, uneven residual stresses are present inside, which are significant factors that lead to the instability of the cylinder shape and deformation. Moreover, during tempering, atoms gain sufficient energy to diffuse, reducing lattice distortion and thereby releasing residual stresses, which creates favorable conditions for correction. At the beginning of the tempering correction process, when external pressure is applied to the cylinder, it undergoes elastic deformation. At this stage, the material follows Hooke's law, where stress is proportional to strain. As the pressure from the pressure block gradually increases, the stress on the cylinder increases correspondingly. During the elastic deformation phase, the amount of deformation is relatively small and fully reversible. The atoms within the material only move slightly around their equilibrium positions, and once the external force is removed, the atoms return to their original positions, causing the cylinder to revert to its initial form. In the transition

phase between elastic and plastic deformation, as the pressure increases, the stress on the cylinder approaches or may exceed the material's yield strength. At this point, part of the material begins to enter the plastic deformation stage, while the other part remains in the elastic deformation stage. On a microscopic level, the crystal structure of the material starts to undergo changes. When the stress reaches the yield strength, dislocations within the crystal lattice begin to move, leading to plastic deformation. However, because some of the material remains elastic, these elastic portions constrain the plastic deformation of the other regions.

Once the pressure continues to accumulate and exceeds a certain critical point, the majority of the material enters the plastic deformation stage. At this stage, the material no longer follows Hooke's law, and unloading will not fully restore the cylinder to its original shape. As plastic deformation continues, the deformation rate increases significantly, and dislocations within the material proliferate, move, and interact, forming complex dislocation networks. The interactions between dislocations make the material's deformation increasingly irreversible, which macroscopically manifests as noticeable changes in the cylinder's shape. During this stage, the tempering temperature significantly influences plastic deformation. Higher tempering temperatures enhance the material's plasticity, making the deformation process smoother.

The correction deformation of the cylinder relies on the elastic-plastic deformation mechanism of the material. Figure 10 depicts the simulation cloud for different phases as time varies. Figure 10(a) shows the simulation cloud of the briquette just lowered to the specified position. Figure 10(b) shows the simulation cloud of final position of the briquette. Figure 11 represents the deformation process when a 45-degree jig is used, while Figure 12 represents the process with a semicircular jig. In the diagrams, the period from 0-1s corresponds to the downward pressure application at different depths, 1–300s represents the heating stage, and 301–600s is the cooling phase, where the pressure block has already been removed from the cylinder surface. It is observed that, with increasing downward pressure, the relative rebound amount decreases. However, during the cooling phase after the pressure block is removed, the rebound rate at point A varies. Notably, for different pressure blocks and pressures, there is a clear pattern in the rebound rates. The rebound rate for the semicircular pressure block is higher than that for the 45-degree jig, and for the same pressure block, as the downward pressure increases, the rebound rate slightly slows down.

For the same jig under different downward pressures, the main factors affecting rebound rate are the magnitude of the pressure and the rate at which it is applied. If the downward pressure is too high, significant plastic deformation occurs, leading to less stored elastic strain

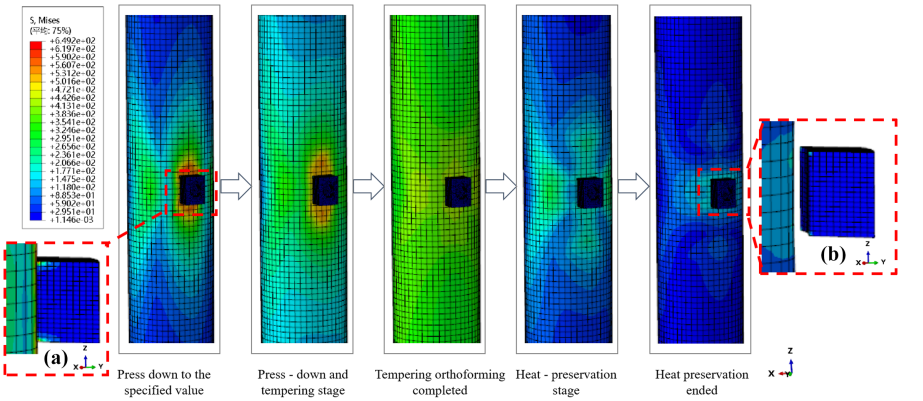


**Figure 10.** Cylinder simulation stress map. Source: Authors' own work

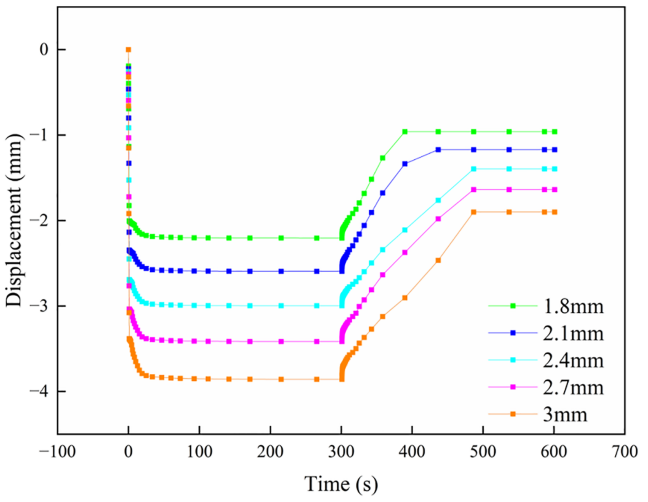


**Figure 11.** Displacement of point A in the *y*-axis direction at different downward pressures (45-degree tooling). Source: Authors' own work

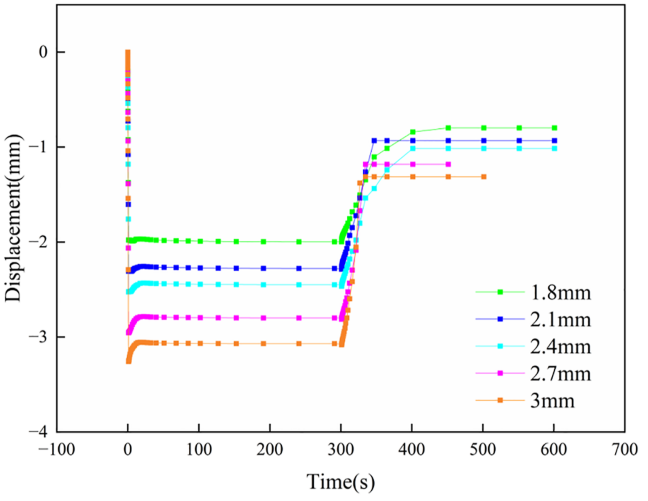


**Figure 12.** Displacement of point A in the *y*-axis direction at different downward pressures (semi-circular tooling). Source: Authors' own work

energy and consequently slower rebound rates. The loading rate is also crucial; fast loading may cause uneven stress distribution within the material, resulting in more localized plastic deformation. When the external force is removed, this uneven stress distribution affects the rebound rate.

When the same downward pressure is applied with different jigs, the contact area between the jig and the cylinder becomes the key factor. Smaller contact areas may lead to stress concentration, causing material in localized regions to reach yield strength faster and undergo plastic deformation. After correction, this localized plastic deformation will affect the rebound

rate. If the jig has point contact, plastic deformation near the contact point is more significant, which may limit rebound in that region, while rebound in surrounding areas occurs more quickly, resulting in uneven overall rebound rates.

In summary, the rebound rate at point A decreases with increasing downward pressure and increases with larger contact areas between the jig and the cylinder.

### *3.4 Deformation amount simulation prediction*

As discussed above, despite validating the accuracy of the simulation model, discrepancies still exist between experimental and simulation results. This could be attributed to measurement errors during experimentation due to manual handling or inaccurate instruments. Additionally, the simulation model used in the finite element software might be overly idealized compared to the actual complex correction process, which prevents a perfect replication of real-world conditions. However, a comparison between the simulation and the actual process shows that the results are quite close. In practical applications, this simulation can play a positive role in guiding the cylinder correction process, effectively improving the first-pass forming rate, reducing production costs, and minimizing unnecessary losses.

Through simulation of a large dataset, this paper plotted the fitting curves for downward pressure versus rebound amount for both the 45-degree and semicircular jigs, as shown in Figures 13 and 14. Here, Figure 13 corresponds to the 45-degree jig, and Figure 14 corresponds to the semicircular jig. The fitting curve equation for the 45-degree jig is: $y = 0.21x + 0.48$, and for the semicircular jig: $y = 0.58x - 0.04$. Using these fitting curves, the cylinder

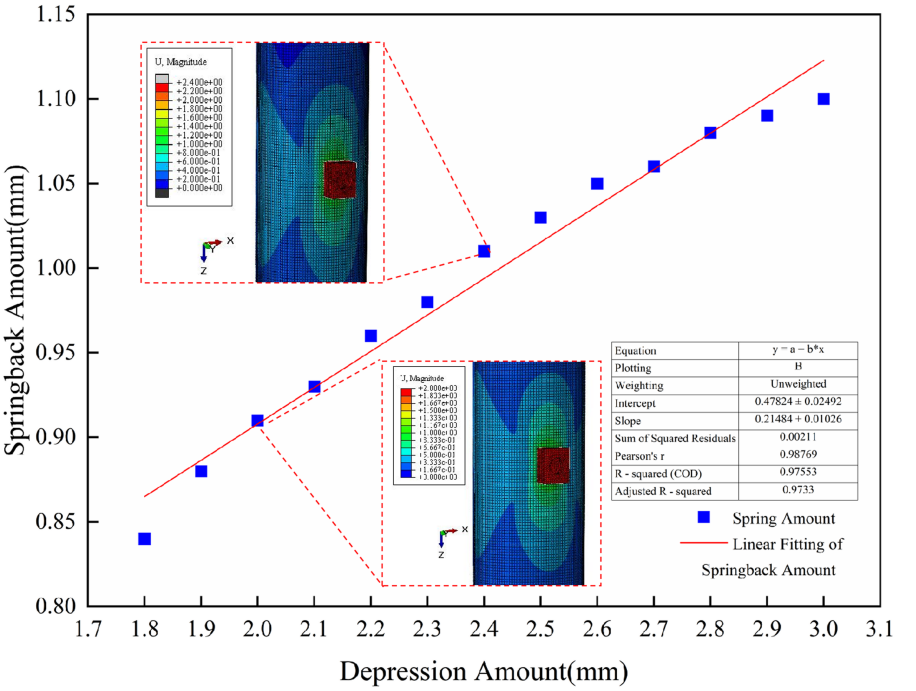


**Figure 13.** Fitting curve of 45° tooling press – down amount and springback amount. Source: Authors' own work

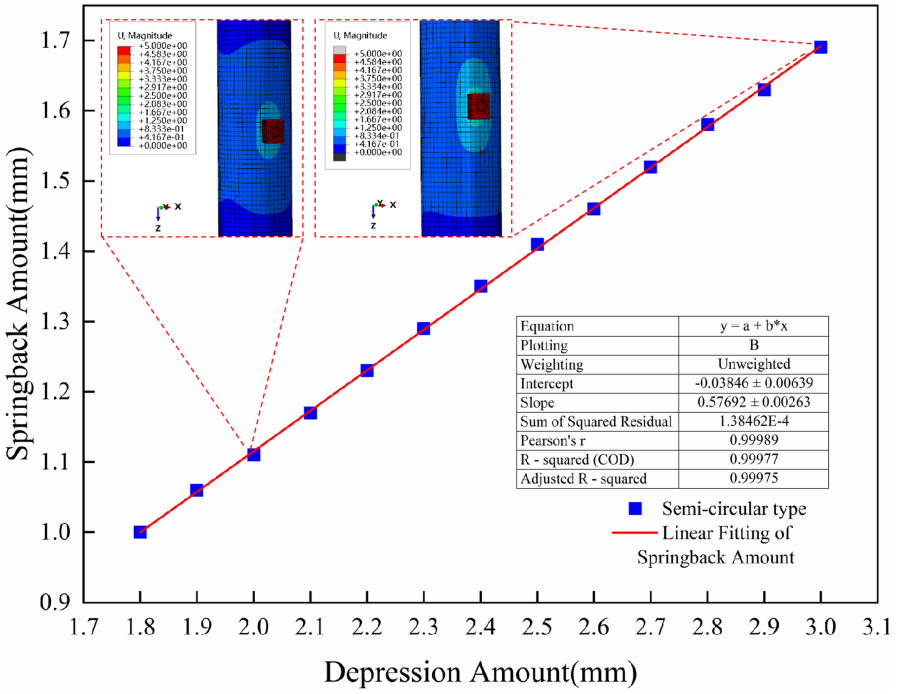


**Figure 14.** Fitting curve of the pressing amount of the semi-circular tooling and the springback amount. Source: Authors' own work

correction process can be predicted, significantly reducing trial-and-error costs and improving work efficiency. This also provides valuable reference material for the industry.

## 4. Conclusions

This study uses the finite element simulation software to simulate the correction process of a cylinder under different conditions and compares the results with experimental data. The following conclusions can be drawn:

(1) Although there are discrepancies between the simulation data and experimental results, these differences do not affect the guiding role of the simulation in the actual correction process.

(2) Under different jig conditions, a smaller contact area results in less rebound after tempering correction due to factors such as stress concentration, reduced elastic strain energy storage, minimal friction interference, and a concentrated thermal influence zone. Conversely, a larger contact area leads to more rebound.

(3) The correction deformation of the cylinder is based on the elastic-plastic deformation mechanism of materials. Under the same contact area, the larger the downward pressure, the smaller the relative rebound amount and rebound rate. Conversely, for the same downward pressure, jigs with larger contact areas result in faster rebound rates.

(4) By organizing a large amount of simulation data and fitting it into a curve, guidance for the actual production process can be provided, allowing for the optimization and prediction of the cylinder correction process.

**References**

Esterl, R., Sonnleitn, M., Gschöpf, B. and Schnitze, R. (2019), "Influence of V and Nb micro-alloying on direct quenched and tempered ultra-high strength steels", *Steel Research International*, Vol. 90 No. 6, 800640, doi: 10.1002/srin.201800640.

Fan, Z., Ge, S., Yue, Z., Yu, R., Li, B., Jiao, J., Liu, J. and Zhang, Q. (2024), "Dynamic response of clamped metallic thin-walled cylindrical shells under lateral shock loading", *Thin-Walled Structures*, Vol. 200, 111922, doi: 10.1016/j.tws.2024.111922.

Hannula, J., Porter, D., Kaijalainen, A., Somani, M. and Kömi, J. (2019), "Mechanical properties of direct-quenched ultra-high-strength steel alloyed with molybdenum and niobium", *Metals*, Vol. 9 No. 3, p. 350, doi: 10.3390/met9030350.

Keränen, L., Nousiainen, O., Javaheri, V., Kaijalainen, A., Pokka, A., Keskitalo, M., Niskanen, J. and Kurvinen, E. (2022), "Mechanical properties of welded ultrahigh-strength S960 steel at low and elevated temperatures", *Journal of Constructional Steel Research*, Vol. 198, 107517, doi: 10.1016/j.jcsr.2022.107517.

Lassi, K., Matti, K. and Juhani, N. (2021), "Ultrahigh-strength steels at elevated temperatures", *Journal of Constructional Steel Research*, Vol. 183, 106739, doi: 10.1016/j.jcsr.2021.106739.

Li, K., Wang, P., Liu, G., Yuan, P. and Zhang, Q. (2016), "Development of simulation system for large H-beam hot rolling based on ABAQUS", *International Journal of Advanced Manufacturing Technology*, Vol. 85 Nos 5-8, pp. 1649-1663, doi: 10.1007/s00170-015-8015-0.

Li, F., Shi, W., Tu, Y. and Zhang, H. (2023a), "Automated methods for indoor point cloud preprocessing: coordinate frame reorientation and building exterior removal", *Journal of Building Engineering*, Vol. 76, 107270, doi: 10.1016/j.jobe.2023.107270.

Li, R., He, W. and Liu, S. (2023b), "Three-dimensional point cloud data pre-processing for the multi-source information fusion in aircraft assembly", *Applied Sciences*, Vol. 13 No. 8, p. 4719, doi: 10.3390/app13084719.

Li, C., Wang, K., Piao, Y., Cui, H., Zakharov, O., Duan, Z., Zhang, F., Yan, Y. and Geng, Y. (2024), "Surface micro-morphology model involved in grinding of GaN crystals driven by strain-rate and abrasive coupling effects", *International Journal of Machine Tools and Manufacture*, Vol. 201, 104197, doi: 10.1016/j.ijmachtools.2024.104197.

Li, C., Liu, G., Gao, C., Yang, R., Zakharov, O., Hu, Y., Yan, Y. and Geng, Y. (2025), "Atomic-scale understanding of graphene oxide lubrication-assisted grinding of GaN crystals", *International Journal of Mechanical Sciences*, Vol. 286, 109934, doi: 10.1016/j.ijmecsci.2025.109934.

Lu, K., Chen, X., Pang, X. and Liu, F. (2024), "Time-varying vibration characteristics and surface topography of thin-walled cylinders during machining operations", *Measurement*, Vol. 232, 114725, doi: 10.1016/j.measurement.2024.114725.

Mishnev, R., Borisova, Y., Kniaziuk, T., Gaidar, S. and Kaibyshev, R. (2023), "Quench and tempered embrittlement of ultra-high-strength steels with transition carbides", *Metals*, Vol. 13 No. 8, p. 1899, doi: 10.3390/met13081399.

Pei, H., Zhang, P., Du, S. and Ming, L. (2023), "A point cloud preprocessing method for complicated thin-walled ring parts with irregular section", *Measurement*, Vol. 214, 112807, doi: 10.1016/j.measurement.2023.112807.

Rong, Z., Xu, D. and Feng, F. (2018), "Plastic behavior of circular steel tubes subjected to low-velocity transverse impact", *International Journal of Impact Engineering*, Vol. 114, pp. 1-19, doi: 10.1016/j.ijimpeng.2017.12.003.

Tian, S., Liu, Z., Fu, R., Dong, C. and Wang, X. (2022), "Effect of organizational evolution on the stress corrosion cracking of the Cr-Co-Ni-Mo series of ultra-high strength stainless steel", *Mater*, Vol. 15 No. 2, p. 497, doi: 10.3390/ma15020497.

Wang, X., zhao, B., Ding, W., Pu, C., Wang, X., Peng, S. and Ma, F. (2022), "A short review on machining deformation control of aero-engine thin-walled casings", *International Journal of Advanced Manufacturing Technology*, Vol. 121 Nos 5-6, pp. 2971-2985, doi: 10.1007/s00170-022-09546-w.

Wang, L., Chen, Y., Song, W. and Xu, H. (2024), "Point cloud denoising and feature preservation: an adaptive kernel approach based on local density and global statistics", *Sens*, Vol. 24 No. 6, p. 1718, doi: 10.3390/s24061718.

Xu, C., Yu, M. and Wu, H. (2018), "Simulation analysis of quenching process of high strength steel based on ABAQUS", *IOP Conference Series: Materials Science and Engineering*, Vol. 423, 012075, doi: 10.1088/1757-899x/423/1/012075.

Yang, C., Li, Z., Xu, P., Huang, H., Huo, Y. and Wei, Y. (2024), "Prediction method of impact deformation mode based on multimodal fusion with point cloud sequences: applied to thin-walled structures", *AEI*, Vol. 59, 102238, doi: 10.1016/j.aei.2023.102238.

Zhang, Y., Zhan, D., Qi, X. and Jiang, Z. (2019), "Effect of tempering temperature on the microstructure and properties of ultrahigh-strength stainless steel", *Journal of Materials Science and Technology*, Vol. 35 No. 7, pp. 1240-1249, doi: 10.1016/j.jmst.2019.01.009.

Zhang, Z., Pang, M. and Teng, C. (2022), "Research on measurement of tooth profile parameters of synchronous belt based on point cloud data", *Sens.*, Vol. 22 No. 17, p. 6372, doi: 10.3390/s22176372.

Zheng, Z., Zha, B., Zhou, Y., Huang, J., Xuchen, Y. and Zhang, H. (2022), "Single-stage adaptive multi-scale point cloud noise filtering algorithm based on feature information", *Remote Sensing*, Vol. 14 No. 2, p. 367, doi: 10.3390/rs14020367.

Zhou, X., Zhang, C., Xu, M., Wu, B. and Zhang, D. (2023), "Prediction of chatter stability in bull-nose end milling of thin-walled cylindrical parts using layered cutting force coefficients", *Applied Sciences*, Vol. 13 No. 11, p. 6737, doi: 10.3390/app13116737.

Zhu, M., Leng, B., Xiao, C., Hou, G., Yao, X. and Li, K. (2022), "Research on fast pre-processing method of tunnel point cloud data in complex environment", *Journal of Physics: Conference Series*, Vol. 2185 No. 1, 012038, doi: 10.1088/1742-6596/2185/1/012038.

Zhuang, K., Wu, Z., Wan, L., Weng, J., Yang, Y., Tian, C., Li, Y. and Liu, Z. (2024), "Investigation of different abrasive jet machining methods applied to milling tool coatings for post-treatment", *Surface and Coatings Technology*, Vol. 491, 131156, doi: 10.1016/j.jmapro.2024.07.089.

**Corresponding author**
Chongjun Wu can be contacted at: wcjunm@dhu.edu.cn